Wide-range-tunable Dirac-cone band structure in a chiral-time-symmetric non-Hermitian system

S. Lin[1,2] and Z. Song[1,*]

[1]*School of Physics, Nankai University, Tianjin 300071, China*

[2]*Science and Technology on Electro-Optical Information Security Control Laboratory, Tianjin 300308, China*

(Received 29 June 2017; published 17 November 2017)

We establish a connection between an arbitrary Hermitian tight-binding model with chiral ($\mathcal{C}$) symmetry and its non-Hermitian counterpart with chiral-time ($\mathcal{CT}$) symmetry. We show that such a non-Hermitian Hamiltonian is pseudo-Hermitian. The eigenvalues and eigenvectors of the non-Hermitian Hamiltonian can be easily obtained from those of its parent Hermitian Hamiltonian. It provides a way to generate a class of non-Hermitian models with a tunable full real band structure by means of additional imaginary potentials. We also present an illustrative example that could achieve a cone structure from the energy band of a two-layer Hermitian square lattice model.

DOI: 10.1103/PhysRevA.96.052121

I. INTRODUCTION

Extra imaginary potentials induce many unusual features even in certain simple or trivial systems, which include quantum phase transition occurred in a finite system [1–20], unidirectional propagation and anomalous transport [4,21–28], invisible defects [29–31], coherent absorption [32] and self-sustained emission [33–37], loss-induced revival of lasing [38], as well as laser-mode selection [39,40]. Most of these phenomena are related to the critical behaviors near exceptional or spectral singularity points. It opens a way for exploring novel quantum states. The basis of such approaches is to seek various non-Hermitian systems with exact solutions. Recently, the graphene-like materials with Dirac cones at the Fermi energy and a number of unique mechanical, electrical, and optical properties have attracted much attention [41]. Its linear-Dirac dispersion makes it an active topic in various research fields. However, for materials in nature, it is very hard to realize experimentally with tuneable parameters. An artificial system, such as photonic simulator, would provide a platform to simulate some aspects in various band structures. Previous efforts mainly focus on the Hermitian systems. A natural question would emerge that whether one can find some artificial materials which have a cone band structure.

In this paper, we consider a method of constructing a variety of non-Hermitian systems which have full real spectra. We focus on the connection between an arbitrary Hermitian tight-binding model with chiral ($\mathcal{C}$) symmetry and its non-Hermitian counterpart with chiral-time ($\mathcal{CT}$) symmetry. We show that such a kind of non-Hermitian Hamiltonian is pseudo-Hermitian. The obtained result indicates that the eigenvalues and eigenvectors of the non-Hermitian Hamiltonian can be easily obtained from those of its parent Hermitian Hamiltonian and the reality of the spectrum is robust to the disorder. It also provides a way to generate a class of non-Hermitian models with a tunable full real band structure by means of additional imaginary potentials. We present an illustrative example, which is a two-layer square lattice model. By adding staggered imaginary potentials, exact result shows that a cone band structure can be achieved.

*songtc@nankai.edu.cn

The remainder of this paper is organized as follows. In Sec. II, we present a general formalism for the solution of an arbitrary non-Hermitian $\mathcal{CT}$-symmetric system. Section III is devoted to present an illustrative example of a two-layer square lattice model. Finally, we present a summary and discussion in Sec. IV.

II. MODEL AND FORMALISM

The main interest of this work is focused on the relation between an arbitrary Hermitian tight-binding model with $\mathcal{C}$ symmetry and a non-Hermitian model which is constructed based on the former by adding additional imaginary potentials. The latter is a non-Hermitian counterpart of the former in the context of this work.

Consider the Hamiltonian of a non-Hermitian tight-binding model

$$H = H_0 + H_\gamma, \tag{1}$$

with

$$H_0 = \sum_{i,j} J_{ij} |i\rangle_{\rm A}\langle j|_{\rm B} + {\rm H.c.}, \tag{2}$$

$$H_\gamma = i\gamma \sum_j (|j\rangle_{\rm A}\langle j|_{\rm A} - |j\rangle_{\rm B}\langle j|_{\rm B}), \tag{3}$$

on a bipartite lattice $\Lambda = 2N$ which can be decomposed into two sublattices $\Lambda_{\rm A}$ and $\Lambda_{\rm B}$. Here we only consider the case with identical sublattice numbers $\Lambda_{\rm A} = \Lambda_{\rm B} = N$ for simplicity. A schematic illustration of the model is presented in Fig. 1(a). The Hamiltonian H_0 has both $\mathcal{C}$ and time-reversal ($\mathcal{T}$) symmetries, i.e.,

$$\mathcal{C} H_0 \mathcal{C}^{-1} = -H_0, \mathcal{T} H_0 \mathcal{T}^{-1} = H_0, \tag{4}$$

where the operators $\mathcal{C}$ and $\mathcal{T}$ are defined as

$$\mathcal{C}|j\rangle_{\rm A} = |j\rangle_{\rm A}, \mathcal{C}|j\rangle_{\rm B} = -|j\rangle_{\rm B}, \tag{5}$$

$$\mathcal{T}\sqrt{-1}\mathcal{T}^{-1} = -\sqrt{-1}. \tag{6}$$

The Hamiltonian H has $\mathcal{CT}$ symmetry, i.e.,

$$\mathcal{C} H \mathcal{C}^{-1} \neq -H, \mathcal{T} H \mathcal{T}^{-1} \neq H, \tag{7}$$

$$\mathcal{CT} H \mathcal{T}^{-1} \mathcal{C}^{-1} = -H. \tag{8}$$

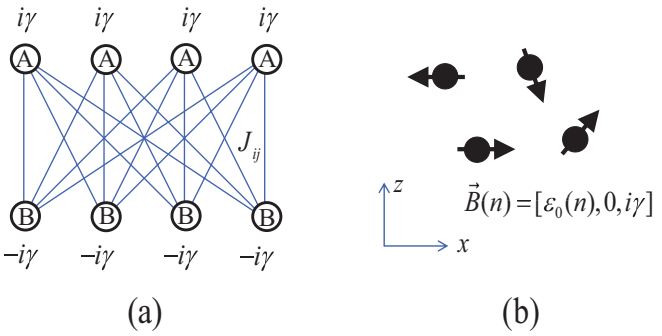

FIG. 1. Schematics for the system with $\Lambda_A = \Lambda_B = 4$ to illustrate the connection between the systems of Eqs. (1) and (15). (a) A bipartite lattice consists of sublattices A and B, which are connected by bond J_{ij} which is across the ith site in sublattice A and the jth site in sublattice B. In the absence of imaginary potentials, i.e., $\gamma = 0$, it has $\mathcal{C}$ symmetry, which ensures that the system has the spectrum $\pm\varepsilon_0(n)$ ($n = 1,2,3,4$). In the presence of imaginary potentials, it has $\mathcal{CT}$ symmetry and becomes a pseudo-Hermitian system. (b) An ensemble of noninteracting half-spins in a complex external magnetic field. It is an equivalent system of (a) when the local magnetic field for spin n has the form $\vec{B}(n)$.

We note that Hamiltonian H_0 has $\mathcal{C}$ symmetry, which is broken in its non-Hermitian counterpart H in the presence of imaginary potentials H_γ. The situation here is a little different from the case associated with parity-time ($\mathcal{PT}$) symmetry, where the combined operator $\mathcal{PT}$ commutes with the Hamiltonian. In quantum mechanics, we say that a Hamiltonian H has a symmetry represented by a operator $\mathcal{U}$ if $[H,\mathcal{U}] = 0$. The word "symmetry" is also used in a different sense in condensed matter physics. We say that a system with Hamiltonian H has chiral symmetry, if $\{H,\mathcal{C}\} = 0$. The physics of $\mathcal{C}$ depends on the model discussed [42–47] . Here we emphasize "chiral symmetry" due to its anticommutation relation with its Hamiltonians. Specifically, the anticommutation relation between operators $\mathcal{CT}$ and H results in the equations

$$H|\psi\rangle = \varepsilon|\psi\rangle, \tag{9}$$

$$H\mathcal{CT}|\psi\rangle = -\varepsilon^*\mathcal{CT}|\psi\rangle. \tag{10}$$

However, the $\mathcal{CT}$ symmetry is like anti-$\mathcal{PT}$ symmetry [46]. Actually, an anti-$\mathcal{PT}$-symmetric Hamiltonian can be simply constructed from a conventional $\mathcal{PT}$-symmetric Hamiltonian by multiplying i. Here the difference and connection between $\mathcal{CT}$ and $\mathcal{PT}$ symmetry has been demonstrated in Table I.

Since the relation $\{\mathcal{CT},H\} = 0$ cannot guarantee operators $\mathcal{CT}$ and H possess a common complete set of eigensates, it is difficult to define the $\mathcal{CT}$ symmetry of a state $|\psi\rangle$. In order to define the $\mathcal{CT}$ symmetry of a state, we consider the operator iH which obeys the relation $[\mathcal{CT},iH] = 0$. Then $\mathcal{CT}$ and H can have a common complete set of eigensates. The $\mathcal{CT}$ symmetry of a state $|\psi\rangle$ is defined as usual, $\mathcal{CT}|\psi\rangle = c|\psi\rangle$. Accordingly, in the exact $\mathcal{CT}$-symmetric region, all the eigenstate obeys $\mathcal{CT}|\psi\rangle = c|\psi\rangle$ and iH has fully real spectrum. For the concerned model, the eigenenergy of H is either real or pure imaginary. When all the eigenstates break the $\mathcal{CT}$ symmetry,

TABLE I. The difference and connection between $\mathcal{CT}$ and $\mathcal{PT}$ symmetry.

$H\|\psi\rangle = \varepsilon\|\psi\rangle$	$\mathcal{PT}$	$\mathcal{CT}$
Symmetry	$[\mathcal{PT},H] = 0$	$\{\mathcal{CT},H\} = 0$
Real ε	$H\mathcal{PT}\|\psi\rangle = \varepsilon\mathcal{PT}\|\psi\rangle$	$H\mathcal{CT}\|\psi\rangle = -\varepsilon\mathcal{CT}\|\psi\rangle$
Imaginary ε	$H\mathcal{PT}\|\psi\rangle = -\varepsilon\mathcal{PT}\|\psi\rangle$	$H\mathcal{CT}\|\psi\rangle = \varepsilon\mathcal{CT}\|\psi\rangle$
	(a)	
$H' = iH$	$\mathcal{PT}$	$\mathcal{CT}$
Symmetry	$\{\mathcal{PT},H'\} = 0$	$[\mathcal{CT},H'] = 0$
Real ε	$H'\mathcal{PT}\|\psi\rangle = -\varepsilon\mathcal{PT}\|\psi\rangle$	$H'\mathcal{CT}\|\psi\rangle = \varepsilon\mathcal{CT}\|\psi\rangle$
Imaginary ε	$H'\mathcal{PT}\|\psi\rangle = \varepsilon\mathcal{PT}\|\psi\rangle$	$H'\mathcal{CT}\|\psi\rangle = -\varepsilon\mathcal{CT}\|\psi\rangle$
	(b)	

i.e., $\mathcal{CT}|\psi\rangle \neq c|\psi\rangle$, the Hamiltonian has fully real spectrum, and $|\psi\rangle$ and $\mathcal{CT}|\psi\rangle$ have the opposite real eigenenergies.

Now we investigate the Hamiltonian H in a pseudospin representation. We will show that H is a pseudo-Hermitian Hamiltonian and there is a simple relation between the spectra of H and H_0. Due to the $\mathcal{C}$ symmetry, the Hamiltonian H_0 can be diagonalized as the form

$$H_0 = \sum_{n=1}^{N} \varepsilon_0(n)(|\varphi_n^+\rangle\langle\varphi_n^+| - |\varphi_n^-\rangle\langle\varphi_n^-|), \tag{11}$$

where $\varepsilon_0(n) > 0$ is the positive energy spectrum with $n \in [1,N]$, and

$$|\varphi_n^\pm\rangle = \frac{1}{\sqrt{2}}(|\phi_n\rangle_A \pm |\phi_n\rangle_B), \tag{12}$$

are eigenstates with eigenenergies $\pm\varepsilon_0(n)$. Here states $|\phi_n\rangle_A$ and $|\phi_n\rangle_B$ are single-particle states with particle probability only distributed on sublattices A and B, respectively. Due to the $\mathcal{C}$ symmetry of H_0, it is easy to check that $|\varphi_n^-\rangle = \mathcal{C}|\varphi_n^+\rangle$. One can express the Hamiltonian in the representation of pseudo spins

$$H_0 = \sum_{n=1}^{N} \varepsilon_0(n)\sigma_n^x, \tag{13}$$

where

$$\sigma_n^x = |\phi_n\rangle_B\langle\phi_n|_A + |\phi_n\rangle_A\langle\phi_n|_B \tag{14}$$

is the x component of the Pauli matrix. Accordingly, we could rewrite the Hamiltonian H as the form

$$H = \sum_{n=1}^{N} \vec{B}(n)\cdot\vec{\sigma}_n, \tag{15}$$

which describes an ensemble of noninteracting half-spins in a complex external magnetic field. Here the field and the Pauli matrices are

$$\vec{B}(n) = [\varepsilon_0(n),0,i\gamma], \tag{16}$$

$$\sigma_n^z = |\phi_n\rangle_A\langle\phi_n|_A - |\phi_n\rangle_B\langle\phi_n|_B, \tag{17}$$

$$\sigma_n^y = i|\phi_n\rangle_B\langle\phi_n|_A - i|\phi_n\rangle_A\langle\phi_n|_B. \tag{18}$$

Based on this analysis, the eigenstates and eigenenergies of Hamiltonian H are

$$|\psi_n^{\pm}\rangle = \frac{1}{\sqrt{\Omega_{\pm}}}(|\phi_n\rangle_{\rm A} \pm e^{\mp i\theta}|\phi_n\rangle_{\rm B}), \tag{19}$$

$$\varepsilon(n) = \pm\sqrt{[\varepsilon_0(n)]^2 - \gamma^2}, \tag{20}$$

where $\theta = \arccos\sqrt{1-[\gamma/\varepsilon_0(n)]^2}$ and the Dirac normalized coefficients are $\Omega_{\pm} = 1 + \exp(\pm 2{\rm Im}\theta)$.

This result has many implications. (i) Non-Hermitian Hamiltonian H is pseudo-Hermitian, since it has either a real spectrum or else its complex eigenvalues always occur in complex conjugate pairs [48]. (ii) It explicitly connects the complete set $\{\varepsilon(n), |\psi_n^{\pm}\rangle\}$ to $\{\pm\varepsilon_0(n), |\varphi_n^{\pm}\rangle\}$. Only an extra phase is added in $|\psi_n^{\pm}\rangle$ from $|\varphi_n^{\pm}\rangle$, which indicates that the two states have the same Dirac probability distribution when $\varepsilon(n)$ is real. (iii) The exceptional points occur at $\gamma = \gamma_{\rm c} = \pm\varepsilon_0(n)$, which correspond to the $\mathcal{CT}$ symmetry breaking of states $|\psi_n^{\pm}\rangle$. It allows a variety of non-Hermitian models with a wide range of disorder parameters to have a full real spectrum and the modulation of band structure is due to the non-Hermiticity. In the next section, we will show its application in an example.

To demonstrate these features, we consider an example model, a generalized non-Hermitian Rice-Mele model, which has been investigated in Refs. [49,50]. The corresponding Hermitian Hamiltonian has the form

$$H_0 = \sum_{j=1}^{N}(J_{2j-1}|j\rangle_{\rm A}\langle j|_{\rm B} + J_{2j}|j\rangle_{\rm B}\langle j+1|_{\rm A}) + {\rm H.c.} \tag{21}$$

with the periodic boundary condition $|2N+1\rangle_{\rm A} = |1\rangle_{\rm A}$. The hopping amplitude between two sublattices is $J_j = 1 + (-1)^j\delta$, where δ is the dimerization factor. The generalized non-Hermitian Rice-Mele Hamiltonian has been completely solved and the obtained result can be recovered by the present method. In this case, we have

$$\varepsilon(k) = \pm\sqrt{[\varepsilon_0(k)]^2 - \gamma^2}, \tag{22}$$

$$\varepsilon_0(k) = 2\sqrt{\delta^2 + (1-\delta^2)\cos^2(k/2)}, \tag{23}$$

with $k = 2\pi n/N$, $n \in [1,N]$. In the absence of γ, the energy gap is 4δ, which determines the exceptional point occurring at $\gamma = \gamma_{\rm c} = \pm 2\delta$ for the non-Hermitian Rice-Mele Hamiltonian. In other words, the energy gap of H_0 protects the $\mathcal{CT}$ symmetry of the eigenstates of H. This is still true in the presence of noise in J_j. In contrast to a $\mathcal{PT}$ symmetric system, the reality of the spectrum for a $\mathcal{CT}$ symmetric one is more robust to the disorder of coupling constants.

III. CONE STRUCTURE

The connection between H_0 and H can be employed to modulate the band structure of H, which has some intriguing properties induced by the non-Hermitian term H_γ. In traditional condensed matter theories, the energy band structure plays a crucial role in the theory of electron conductivity in the solid state and explains why materials can be classified as insulators, conductors, and semiconductors. Moreover, much attention has been paid to the honeycomb lattice [41], which is relevant to high electron mobility and topological phase, as exemplified by the graphene.

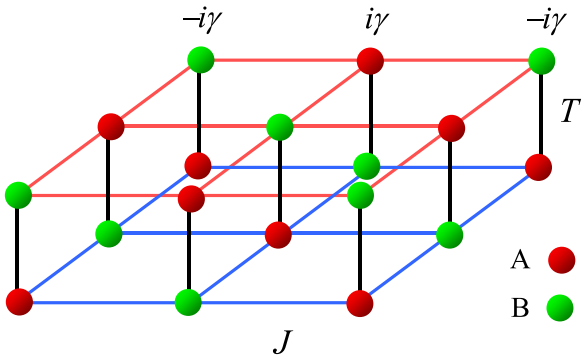

FIG. 2. (a) Schematic illustration of a bilayer square lattice with staggered imaginary potentials. The two sublattices are denoted by A (red) and B (green), respectively. The intra- and interlayer hopping strengths are J and T, respectively. For $\gamma = 0$, the system has both $\mathcal{C}$ and $\mathcal{T}$ symmetries, while nonzero γ breaks the $\mathcal{C}$ symmetry but maintains the $\mathcal{CT}$ symmetry. The additional staggered imaginary potentials make the simple lattice have a tunable cone band structure.

In the Hermitian realm, the band structures of most kinds of systems have been well studied. Nevertheless, non-Hermitian parameters may induce an unusual band structure which is difficult to achieve in a Hermitian system. As an example, Eq. (20) provides a way to accomplish this task that imaginary potentials can deform the shape of a given band structure without altering its topology except the situation when the system contains the exceptional points. In the following, we will present an example which realizes a cone structure on a square lattice.

We consider a bilayer square lattice model which is shown in Fig. 2. The corresponding Hermitian Hamiltonian has the form

$$H_0 = H_1 + H_2 + H_{12}, \tag{24}$$

$$H_\lambda = J\sum_{j,l=1}^{N}|\lambda,j,l\rangle(\langle\lambda,j+1,l| + \langle\lambda,j,l+1|) + {\rm H.c.}, \tag{25}$$

$$H_{12} = T\sum_{j,l=1}^{N}|1,j,l\rangle\langle 2,j,l| + {\rm H.c.}, \tag{26}$$

where $\lambda = 1$ or 2 is the index that respectively labels the position in the top or bottom layers, and (j,l) is the in-plane site index. Parameters J and T of this model are intra- and interlayer hopping strengths. In this paper, we only consider the case of $T > 4J$. And the distribution of imaginary potentials is given as the form

$$H_\gamma = i\gamma\sum_{\lambda=1}^{2}\sum_{j,l=1}^{N}(-1)^{\lambda+j+l}|\lambda,j,l\rangle\langle\lambda,j,l|. \tag{27}$$

The Hamiltonian H_0 can be easily diagonalized via Fourier transformation. Let us consider an individual rung, i.e., two sites with the same in-plane site index on the opposite layers.

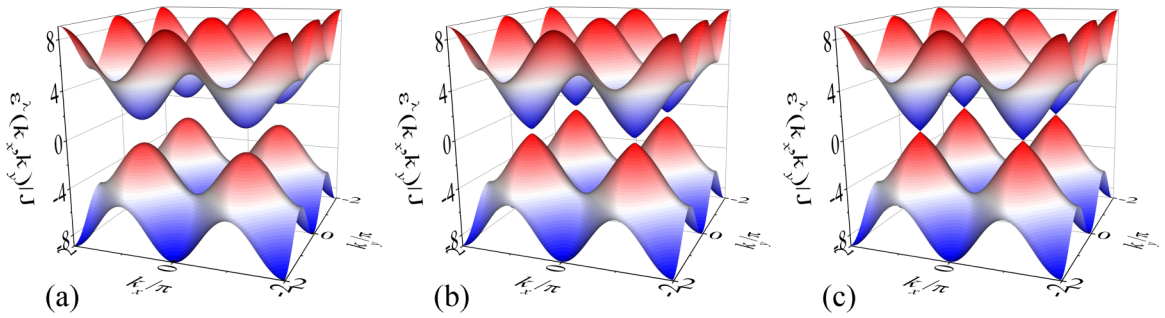

FIG. 3. Three-dimensional plots of band structures of bilayer square lattice with periodic boundary condition. Staggered imaginary potentials $\pm i\gamma$ are applied throughout the lattice and here we set $\lambda = \pm$. The parameters are (a) $T = 5J, \gamma = 0$; (b) $T = 5J, \gamma = 0.98J$; (c) $T = 5J, \gamma = J$. Here the key difference between the cases for (a) and (c) is that the dispersion relation in the bottom of band is quadratic for (a) but linear (cone) for (c). The band structure in case (a) is trivial in the context that Dirac cone in lattice system has been shown to exhibit some novel features. Although a Hermitian system can support Dirac dispersion (e.g., honeycomb lattice), the speed of electron (slope of the cone) is not tunable.

An occupied rung has two possible states that are bond and antibond states. The bond (antibond) state of a rung can only be transited to the bond (antibond) state next to it. Therefore it can be decomposed into two independent single layer square lattices with on-site potentials T and $-T$, respectively. The spectra and eigenvectors are

$$\varepsilon_0^{\pm}(k_x,k_y) = \pm\{2J[\cos(k_x) + \cos(k_y)] + T\} \tag{28}$$

and

$$|\varphi^{\pm}(k_x,k_y)\rangle = \sum_{j,l=1}^{N} \frac{e^{i(k_x j + k_y l)}}{N\sqrt{2}}(|\lambda_A, j, l\rangle \pm |\lambda_B, j, l\rangle), \tag{29}$$

where $\pm$ denotes the two independent single layers, and $k_x = 2n_x\pi/N$, $k_y = 2n_y\pi/N$ with n_x, $n_y \in [1, N]$. States $|\lambda_A, j, l\rangle$ and $|\lambda_B, j, l\rangle$ are the position states of sublattices A and B with the layer labels $\lambda_A = [3 + (-1)^{j+l}]/2$ and $\lambda_B = [3 - (-1)^{j+l}]/2$. This band structure is trivial, but it would be a good parent to construct a cone structure by adding staggered imaginary potentials. Now we consider the corresponding non-Hermitian Hamiltonian $H = H_0 + H_\gamma$. According to the above result, the spectra and eigenvectors of H are

$$\varepsilon^{\pm}(k_x,k_y) = \pm\sqrt{[\varepsilon_0^{\pm}(k_x,k_y)]^2 - \gamma^2} \tag{30}$$

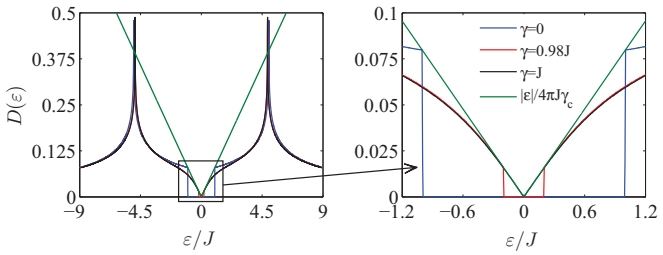

FIG. 4. DOS per unit cell as a function of energy (in units of J) computed from the energy dispersion Eq. (30) with several typical values of $\gamma = 0$ (blue), $0.98J$ (red), J (black). And here we set $T = 5J$. Also shown is a zoom-in of the densities of states close to the zero-energy point, which can be approximated by $D(\varepsilon) \propto |\varepsilon|$. The approximate expression in Eq. (36) is also plotted (solid green) as comparison.

and

$$|\psi^{\pm}(k_x,k_y)\rangle = \sum_{j,l=1}^{N} \frac{e^{i(k_x j + k_y l)}}{N\sqrt{\Omega_{\pm}}}(|\lambda_A, j, l\rangle \pm e^{\mp i\theta}|\lambda_B, j, l\rangle), \tag{31}$$

where

$$\theta = \arccos\sqrt{1 - (\gamma/\varepsilon_0^{\pm})^2} \tag{32}$$

is real when the symmetry is not broken. In the exact $\mathcal{CT}$ -symmetric region, there are local maxima (minima) on the valence (conduction) band at points $(k_x^c, k_y^c) = (\sigma\pi, \sigma'\pi)$ ($\sigma, \sigma' =$ odd). The energy band gap is $2\sqrt{(T-4J)^2 - \gamma^2}$ and the exceptional points occur at $\gamma = \gamma_c = \varepsilon_0(k_x^c, k_y^c) = T - 4J$. In the vicinity of k_c and considering the case $0 < \gamma_c - \gamma \ll J$, we have an approximate relation

$$\frac{(k_x - k_x^c)^2}{a^2} + \frac{(k_y - k_y^c)^2}{b^2} - \frac{(\varepsilon^{\pm})^2}{c^2} = -1, \tag{33}$$

with $c = \sqrt{\gamma_c^2 - \gamma^2}$ and $a = b = c/\sqrt{2J\gamma_c}$, which indicates that the band structure is a hyperboloid of two sheets. For $\gamma = \gamma_c$, it reduces to a Dirac cone. Note that the difference between the cases for $\gamma = 0$ and $\gamma = \gamma_c$ is that the dispersion relation in the bottom of band is quadratic for $\gamma = 0$ but linear (cone) for $\gamma = \gamma_c$. Although a Hermitian system can support Dirac dispersion (e.g., honeycomb lattice), the speed of electron (slope of the cone) is less tunable. In contrast, the group velocity at the linear region for our model is

$$v_g = J\sqrt{2(T/J - 4)}, \tag{34}$$

which indicates that v_g strongly depends on the ratio of J and T ($\gamma_c = T - 4J$), while it only depends on the hopping strength in a honeycomb lattice. In this sense, imaginary extension may make something easier to achieve than that in a Hermitian system. Furthermore, it seems that it has a similar band structure with that of graphene near the zero-energy plane. The difference between them is that the vertices of the cone of graphene are degenerate points, while the ones in the present model are exceptional points. For $\gamma < \gamma_c$, the energy gap and the group velocity are tunable by γ, J, and T. The cone band structures for different γ are plotted in Fig. 3.

We introduce density of states (DOS) to characterize the band structure. DOS is essentially the number of different states at a particular energy level that electrons are allowed to occupy, i.e., the number of electron states per unit volume per unit energy. DOS calculations allow one to capture various electronic properties, such as specific heat, paramagnetic susceptibility, and other transport phenomena of conductive solids. The DOS $D(\varepsilon)$ of energy bands for a square lattice can be expressed as follows:

$$D(\varepsilon) = \frac{1}{4\pi^2} \iint_{\mathrm{B}} \delta[\varepsilon - \varepsilon^{\pm}(k_x,k_y)]dk_x dk_y, \tag{35}$$

which describes the number of states per unit energy per unit cell and therefore the function is properly normalized to $\int_{\mathrm{B}} D(\varepsilon)d\varepsilon = 2$. Due to the symmetry of spectrum, we have $D(\varepsilon) = D(-\varepsilon)$. Here the densities of states for different γ are plotted in Fig. 4. In the vicinity of k_{c} and considering the case $0 \leq \gamma_{\mathrm{c}} - \gamma \ll J$, Eq. (33) allows us to derive an approximate expression for the density of states

$$D(\varepsilon) = \begin{cases} \frac{1}{4\pi J\gamma_{\mathrm{c}}}|\varepsilon|, & |\varepsilon| \geq \sqrt{\gamma_{\mathrm{c}}^2 - \gamma^2} \\ 0, & |\varepsilon| < \sqrt{\gamma_{\mathrm{c}}^2 - \gamma^2} \end{cases}, \tag{36}$$

which is a linear function of energy. We plot this expression in Fig. 4 as comparison. It indicates that $D(\varepsilon)$ shows a semimetallic behavior as that in graphene.

IV. SUMMARY

In conclusion, we have studied the connection between an arbitrary Hermitian tight-binding model with $\mathcal{C}$ symmetry and its non-Hermitian counterpart with $\mathcal{CT}$ symmetry. It has been shown that such a kind of non-Hermitian Hamiltonian is pseudo-Hermitian, providing a way to generate a class of non-Hermitian models with a tunable full real band structure by adding additional imaginary potentials. Based on the exact results, it is found that the eigenvalues and eigenvectors of the non-Hermitian Hamiltonian can be easily obtained from those of its parent Hermitian Hamiltonian. The reality of the spectrum is robust to the disorder due to the protection of energy gap. Furthermore, as an illustrative example, we investigate the band structure of a two-layer square lattice model with staggered imaginary potentials. We find that a tunable cone band structure can be achieved. It should have wide applications in non-Hermitian synthetic graphene-like materials.

ACKNOWLEDGMENT

We acknowledge the support of Chinese Natural Science Foundation (Grant No. 11374163).

[1] M. Znojil, Phys. Lett. B **650**, 440 (2007).
[2] M. Znojil, J. Phys. A **40**, 13131 (2007).
[3] O. Bendix, R. Fleischmann, T. Kottos, and B. Shapiro, Phys. Rev. Lett. **103**, 030402 (2009).
[4] S. Longhi, Phys. Rev. Lett. **103**, 123601 (2009).
[5] S. Longhi, Phys. Rev. B **80**, 235102 (2009).
[6] L. Jin and Z. Song, Phys. Rev. A **80**, 052107 (2009).
[7] M. Znojil, Phys. Rev. A **82**, 052113 (2010).
[8] S. Longhi, Phys. Rev. B **81**, 195118 (2010).
[9] S. Longhi, Phys. Rev. B **82**, 041106(R) (2010).
[10] L. Jin and Z. Song, Phys. Rev. A **81**, 032109 (2010).
[11] Y. N. Joglekar, D. Scott, M. Babbey, and A. Saxena, Phys. Rev. A **82**, 030103(R) (2010).
[12] M. Znojil, J. Phys. A **44**, 075302 (2011).
[13] M. Znojil, Phys. Lett. A **375**, 2503 (2011).
[14] H. Zhong, W. Hai, G. Lu, and Z. Li, Phys. Rev. A **84**, 013410 (2011).
[15] L. B. Drissi, E. H. Saidi, and M. Bousmina, J. Math. Phys. **52**, 022306 (2011).
[16] Y. N. Joglekar and A. Saxena, Phys. Rev. A **83**, 050101(R) (2011).
[17] D. D. Scott and Y. N. Joglekar, Phys. Rev. A **83**, 050102(R) (2011).
[18] Y. N. Joglekar and J. L. Barnett, Phys. Rev. A **84**, 024103 (2011).
[19] D. D. Scott and Y. N. Joglekar, Phys. Rev. A **85**, 062105 (2012).
[20] T. E. Lee and Y. N. Joglekar, Phys. Rev. A **92**, 042103 (2015).
[21] M. Kulishov *et al.*, Opt. Express **13**, 3068 (2005).
[22] S. Longhi, Opt. Lett. **35**, 3844 (2010).
[23] Z. Lin, H. Ramezani, T. Eichelkraut, T. Kottos, H. Cao, and D. N. Christodoulides, Phys. Rev. Lett. **106**, 213901 (2011).
[24] A. Regensburger, C. Bersch, M. A. Miri, G. Onishchukov, D. N. Christodoulides, and U. Peschel, Nature (London) **488**, 167 (2012).
[25] T. Eichelkraut *et al.*, Nat. Commun. **4**, 2533 (2013).
[26] L. Feng *et al.*, Nat. Mater. **12**, 108 (2013).
[27] B. Peng *et al.*, Nat. Phys. **10**, 394 (2014).
[28] L. Chang, Nat. Photonics **8**, 524 (2014).
[29] S. Longhi, Phys. Rev. A **82**, 032111 (2010).
[30] S. Longhi and G. Della Valle, Ann. Phys. (NY) **334**, 35 (2013).
[31] X. Z. Zhang and Z. Song, Ann. Phys. (NY) **339**, 109 (2013).
[32] Y. Sun, W. Tan, H. Q. Li, J. Li, and H. Chen, Phys. Rev. Lett. **112**, 143903 (2014).
[33] A. Mostafazadeh, Phys. Rev. Lett. **102**, 220402 (2009).
[34] S. Longhi, Phys. Rev. B **80**, 165125 (2009).
[35] X. Z. Zhang, L. Jin, and Z. Song, Phys. Rev. A **87**, 042118 (2013).
[36] S. Longhi, Opt. Lett. **40**, 5694 (2015).
[37] X. Q. Li, X. Z. Zhang, G. Zhang, and Z. Song, Phys. Rev. A **91**, 032101 (2015).
[38] B. Peng *et al.*, Science **346**, 328 (2014).
[39] L. Feng, Z. J. Wong, R.-M. Ma, Y. Wang, and X. Zhang, Science **346**, 972 (2014).
[40] H. Hodaei, M. A. Miri, M. Heinrich, D. N. Christodoulides, and M. Khajavikhan, Science **346**, 975 (2014).

[41] A. H. Castro Neto *et al.*, Rev. Mod. Phys. **81**, 109 (2009).
[42] J. K. Asbóth, L. Oroszlány, and A. Pályi, *Band Structure and Edge States in One and Two Dimensions*, Lecture Notes in Phys. 919 (Springer International Publishing, Switzerland, 2016).
[43] S. Malzard, Charles Poli, and Henning Schomerus, Phys. Rev. Lett. **115**, 200402 (2015).
[44] H. Guo and S. Chen, Phys. Rev. B **91**, 041402(R) (2015).
[45] L. Li and S. Chen, Phys. Rev. B **92**, 085118 (2015).
[46] P. Peng, W. Cao, C. Shen, W. Qu, J. Wen, L. Jiang, and Y. Xiao, Nat. Phys. **12**, 1139 (2016).
[47] Tony E. Lee, Phys. Rev. Lett. **116**, 133903 (2016).
[48] A. Mostafazadeh, J. Math. Phys. **43**, 205 (2002).
[49] W. H. Hu, L. Jin, Y. Li, and Z. Song, Phys. Rev. A **86**, 042110 (2012).
[50] S. Lin, X. Z. Zhang, and Z. Song, Phys. Rev. A **92**, 012117 (2015).